Progress In Electromagnetics Research, Vol. 111, 229–251, 2011

PO/MEC-BASED SCATTERING MODEL FOR COMPLEX OBJECTS ON A SEA SURFACE

A. Bausssard, M. Rochdi, and A. Khenchaf

E^3I^2 Laboratory, ENSIETA
2 rue François Verny, Brest 29806, France

Abstract—In this contribution a model based on asymptotic methods is proposed to compute the scattered field from complex objects on a sea surface. The scattering model combines the geometrical optics, the physical optics and the method of equivalent currents. It includes the shadowing effects and multiple-bounce up to order 3. This model is used, in the following, for Radar Cross Section (RCS) estimation and to generate Synthetic Aperture Radar (SAR) raw data for imaging applications. The theoretical aspects are reviewed in this paper and the proposed model is detailed. Numerical results are provided to validate the approach through the computation of RCS for canonical objects and complex scenes. Both the bistatic and the monostatic configurations are studied in this work. Finally some first results dealing with SAR imaging of objects on a sea surface are provided. These images are constructed from the simulated raw data thanks to a chirp scaling-based algorithm.

1. INTRODUCTION

The development of efficient electromagnetic simulators for radar signal simulations or Radar Cross Section (RCS) computation has been of interest for many years. Useful techniques have already been developed to provide realistic results. They can be based on exact methods (integral equations, method of moments ...) or approximate approaches. One can refer to commercial or non commercial software such as XPATCH [1], GRECO [2], FEKO, XFDTD ...

Exact methods are unfortunately not efficient for the moment to calculate the scattered field from a large tridimensional complex object or scene. That is why most simulators are based on asymptotic

Received 30 August 2010, Accepted 31 October 2010, Scheduled 8 December 2010
Corresponding author: Alexandre Baussard (alexandre.baussard@ensieta.fr).

methods. They can use or combine the geometrical optics, the geometrical theory of diffraction (GTD), the physical optics, the physical theory of diffraction, etc. [3–6].

Over the last few years, studies have focused on the introduction of targets in an environment; mostly a rough surface [7–12]. The proposed work falls within this area. It deals with the computation of the scattered field from a complex scene composed of a target floating on a realistic sea surface. The main goal of our project is to generate Synthetic Aperture Radar (SAR) raw data and to construct the corresponding SAR images for maritime surveillance applications (see Figure 1). We believe that few works have already been published dealing with a global imaging radar system (from the model to the SAR processing) of complex scenes and this is the interest of this paper.

This kind of model can be of interest for testing new detection and classification methods or to design optimal operating configurations for maritime surveillance or marine remote sensing. Other works in this area deal with, for example, the analysis of SAR polarimetry for target classification [13], the simulation of SAR images through reflectivity maps [14], or generating of image database of ground targets using commercial simulators [12].

In this contribution, in order to model the scattered field by a complex scene, a combination of geometrical optics, physical optics and the method of equivalent currents has been used. The considered model also includes the shadowing and multi-path effects for more accuracy. This model can be seen as an electromagnetic tool for RCS evaluation and for generating radar signals in maritime environments

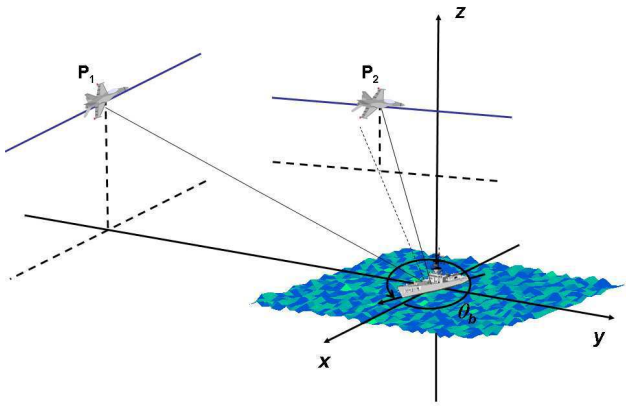

Figure 1. Bistatic SAR imaging setup.

such as SAR raw data for radar imaging applications. Of course the proposed work takes advantage of previous contributions dealing with the modeling of bistatic SAR systems for imaging point target or simplified objects [15, 16] and maritime scenes [17, 18]. The new aspect in this contribution is the introduction of complex objects in the maritime environment.

In Section 2 the considered asymptotic methods are briefly reviewed and the proposed model is described. Numerical RCS results are provided to show the validity of the developed model. Section 3 introduces the scattering model for the maritime surface. In Section 4 a SAR application is proposed for imaging objects floating on a sea surface. Finally concluding remarks end the paper.

2. SCATTERED FIELD MODELING

The computation of the scattered field by complex targets involves different scattering mechanisms such as specular reflection, diffraction at edges, multiple scattering, shadowing effects, etc. An illustration of these phenomena is given in Figure 2.

In this contribution, in order to model the scattered field from a target, the geometrical optics, the physical optics and the method of equivalent currents are considered. These asymptotic methods can be used in the high frequency region of electromagnetic scattering (i.e., the object needs to be larger than the wavelength). Of course, they do not allow the phenomena represented in Figure 2 to be modeled, but they provide a suitable approximation for a weak computational burden in comparison with exact methods. Moreover, for RCS accuracy, the proposed model includes the shadowing effects and multiple-bounce (up to 3).

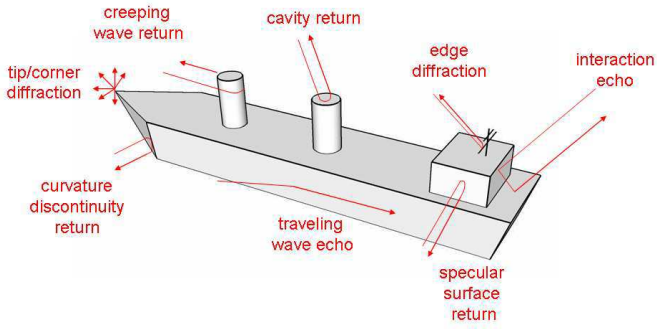

Figure 2. Target RCS contributors.

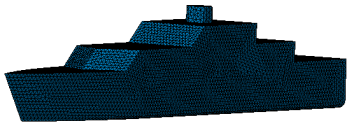

Figure 3. Target composed of triangular patches.

The computation of the considered asymptotic methods needs to geometrically describe the target or the scene. In this way, a surface model of the scene made of triangular elements is considered. To generate the target, the software CATIA has been used. Figure 3 gives an example of a discretized target.

2.1. Geometrical Optics

In Geometrical Optics (GO), it is assumed that the radar energy propagates along ray paths, governed by Fermat's principle. When the ray interacts with a surface, the angle of the scattered ray, measured from the surface normal, is equal to the angle of the incident ray (specular reflection).

2.2. Physical Optics

The initial point of Physical Optics (PO) is the surface currents produced by an incoming electromagnetic wave ($\vec{E}_i$, $\vec{H}_i$). The induced magnetic ($\vec{J}_m$) and electric ($\vec{J}_e$) currents are given by

$$\vec{J}_m = -\hat{n} \times \vec{E}, \qquad \vec{J}_e = \hat{n} \times \vec{H}, \tag{1}$$

where $\hat{n}$ is the unit vector normal to the surface, and $\vec{E}$ and $\vec{H}$ are respectively the total electric and magnetic fields at the surface.

If the source illuminating the target is at a far enough distance, then the incident field can be taken as a plane wave. Following the configuration in Figure 4, the scattered field from the illuminated surface S is given by

$$\vec{E}_s = \frac{jk\mathrm{e}^{-jkR}}{4\pi R} \int_S \left[\hat{k}_s \times (\eta \hat{k}_s \times \vec{J}_e + \vec{J}_m)\right] \mathrm{e}^{-jk\hat{k}_s.\vec{r}} \mathrm{d}s, \tag{2}$$

where k is the wavenumber; R is the distance between the center of the referential and the receiver; $\hat{k}_i$ and $\hat{k}_s$ are respectively the unit directional vectors of the incident and scattering electromagnetic wave. η is the impedance of the medium and $\vec{r}$ is the position vector of a point in S. The integration in Equation (2) can be solved following [19].

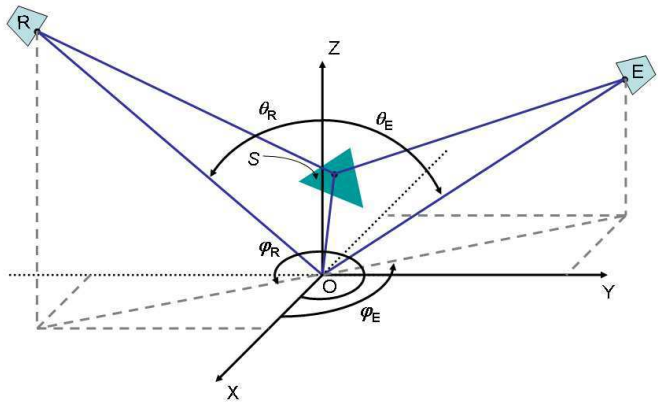

Figure 4. Configuration for the PO computation of the scattered field from a triangular patch.

Notice that the angles used in the following are defined according to Figure 4 and for the monostatic case $\varphi_E = \varphi_R = \varphi$ and $\theta_E = \theta_R = \theta$.

2.3. Method of Equivalent Currents

To improve the PO solution and take into account the diffraction by edges, the Method of Equivalent Currents (MEC) has been proposed by Michaeli [5, 20, 21]. The MEC describes the source of the field in terms of fictitious equivalent electric and magnetic currents along the edge.

According to the MEC and using the local referential in Figure 5, the scattered field by an edge C is given by the radiation integral [5]

$$\vec{E}_d \approx \frac{jk}{4\pi R} \int_C \left[\eta I \hat{k}_s \times \left[\hat{k}_s \times \hat{t} \right] + M \hat{k}_s \times \hat{t} \right] \mathrm{e}^{-jk\hat{k}_s . \vec{r}'} \mathrm{d}l, \qquad (3)$$

where $\vec{r}'$ is the position of a point on C, $\hat{t}$ is the tangent unit vector to the edge, $\vec{I} = I\hat{t}$ and $\vec{M} = M\hat{t}$ are the electric and magnetic equivalent currents, respectively. Figure 5 shows the main referential related to Face 1 of the wedge to compute the scattered field. The dashed lines are the projections of the directions of incidence and observation on the XY-plane. $N\pi$ is the exterior wedge angle (it is assumed that $N > 1$).

Notice that to compute this scattered field, one needs to find the edges of the target. A simple criterion against the angle between two adjacent patches can be used.

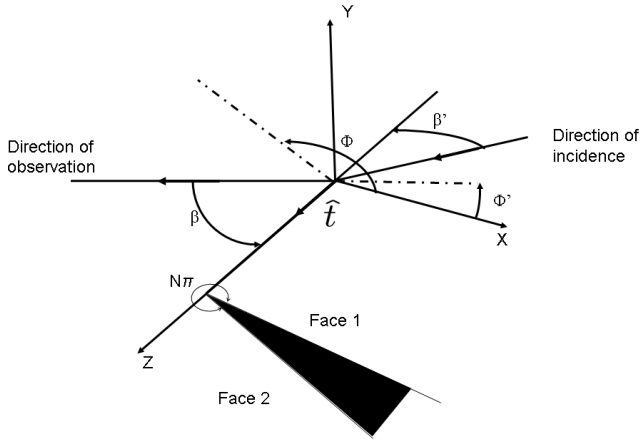

Figure 5. Local referential for the MEC computation.

2.4. Shadowing Effects

Shadowing is introduced to eliminate the effects of the irrelevant scattering sources. Thus, one needs to identify the triangles of the scene which are visible from the emitter and the receiver at each acquisition time. To find the illuminated facets, an algorithm combining backface culling and a Z-buffer-based approach has been developed.

Backface culling is the process by which triangles that are not facing the emitter or the receiver are removed. This is done by comparing the triangle's surface normal with the position of the emitter or the receiver. It is a simple and very fast approach. The Z-buffer-based approach leads to the suppression of the triangles of the scene which are not visible from the emitter or the receiver by using depth-information.

2.5. Multiple-bounce

The possible multiple-bounce scattering mechanisms must be evaluated in order to obtain a suitable model. In the proposed model, one can consider up to 3-bounce (which is necessary for complex targets presenting trihedral geometries).

Basically, the idea is to project each facet reach by a ray in the specular direction (see Figure 6). If at least one of the specular rays coming from each node of the current facet cuts another facet, this means that multiple-bounce exists. In this case, one projects the current facet. If the three vertex of the projected triangle do not belong

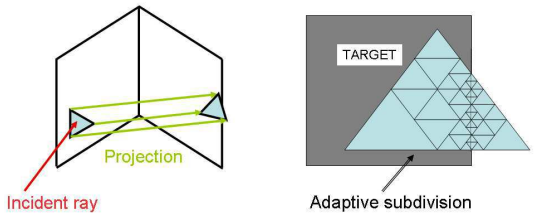

Figure 6. multiple-bounce and adaptive subdivision.

to the same plane surface of the target, in this case, a subdivision of the projected triangle into smaller triangles (see Figure 6) is performed in order to find the illuminated area. The same method is applied to find the third-order bounce.

Finally, for a double-bounce, the scattered field is computed as follows: first geometrical optics is used to find the field which reaches the first and the second facet. Then, the scattered field (from the second facet to the receiver) is computed using physical optics.

2.6. Numerical Results and Validation

In order to validate the considered model, canonical objects are considered in this part. From the scattered field, the radar cross section of the target is computed and compared with results obtained using FEKO software.

Notice that as the targets have been meshed with triangular patches, that for a given incident direction, the total scattered field is the sum of all the scattered fields from the illuminated patches.

2.6.1. RCS of a Trihedral

This target is considered in order to show that multiple reflections up to order 3 are taken into account in the proposed model.

The trihedral dimensions and the monostatic configuration, based on [22], are described in Figure 7.

Figure 8 shows the monostatic RCS obtained with our model and given by FEKO (Method of Moment — MoM) at 10 GHz, for $\theta = 66°$ and $\varphi = 0°$ to $90°$ and for both polarizations. The results obtained using our model are very close to those obtained using FEKO and those proposed in [22].

Figure 9 shows the bistatic RCS obtained for both polarizations with our model and given by FEKO (MoM) at 10 GHz, for a fixed emitter at ($\theta_E = 45°$, $\varphi_E = 45°$) and a moving receiver along $\theta_R = 45°$

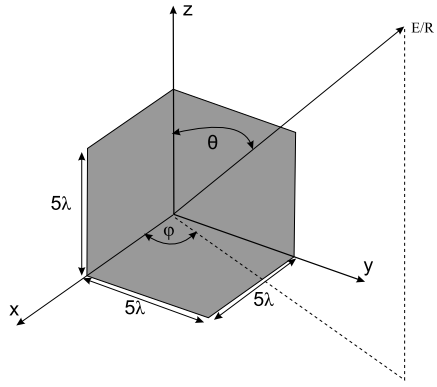

Figure 7. Trihedral setup.

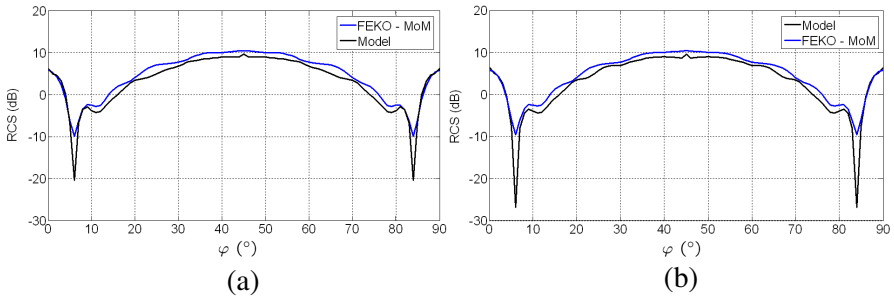

Figure 8. Monostatic RCS of a trihedral (a) *hh*-polarization and (b) *vv*-polarization.

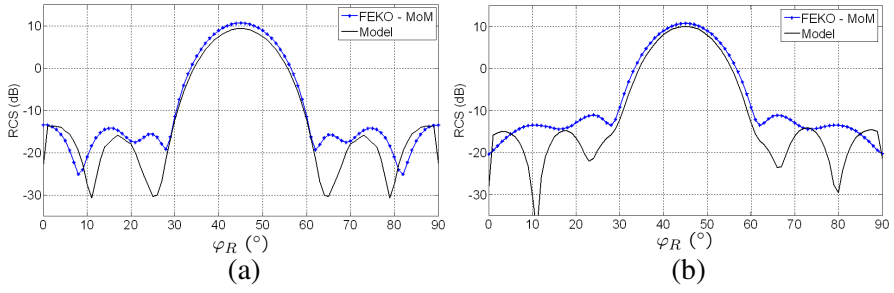

Figure 9. Bistatic RCS of a trihedral (a) *hh*-polarization and (b) *vv*-polarization.

and $\varphi_R = 0°$ to $90°$. The results obtained using our model are very close to those obtained using FEKO in the area $\varphi_R = 28°$ to $62°$. Outside this area, our results show significant differences. They can be explained by multiple reflections which are higher than order 3 (not taken into account in our model). They can also be explain by diffraction at edges after multiple bounces. Indeed our model only includes direct diffraction at edges.

Our goal being to design a scatter model realistic enough to generate radar signals to test and develop imaging or detection applications, the results obtained with our model seems to show sufficient accuracy.

2.6.2. RCS of a Complex Target Made of Canonical Objects

The last target is composed of canonical objects (see Figure 10). This target can be classified as a complex target, even if its design seems simple, since it includes multiple-bounce, shadow areas, diffraction by edges, cross-polarization effects ...

For this target, the bistatic configuration is considered: the emitting antenna is fixed at ($\varphi_E = 90°$, $\theta_E = 45°$) and the receiving antenna move along $\varphi_R = 90°$ and $\theta_R = -90°$ to $90°$. The operating frequency is 2 GHz.

Figure 11 shows the RCS results obtained using our model and FEKO (MoM method). As expected, since our model does not take into account all the physical phenomena which take place during the interaction between the electromagnetic wave and the object, our RCS results show differences with the FEKO's method of moment. However, globally these results show good accuracy in the RCS form evolution according to θ_R.

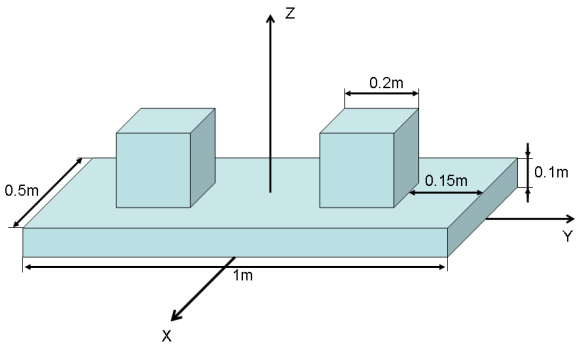

Figure 10. Dimensions of the target composed of canonical objects.

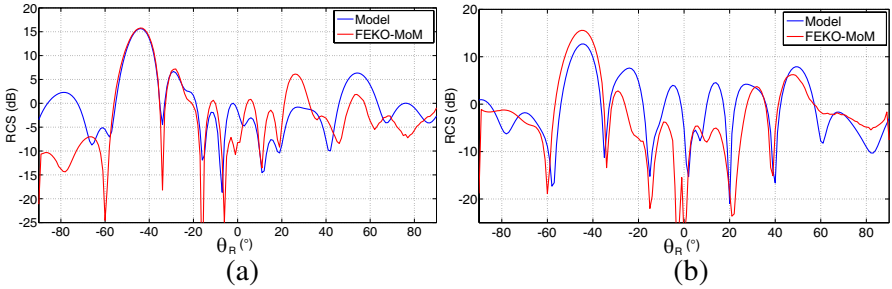

Figure 11. Bistatic RCS of a complex object (a) *hh*-polarization and (b) *vv*-polarization.

3. RCS OF MARITIME SCENES

In previous works [17, 18] dealing with ship wake modeling in a bistatic SAR configuration, the scattered field from the sea surface was computed using a so-called semi-deterministic, semi-statistical facet-based version of a two scales method. In this contribution, the scattered field will be computed from a deterministic sea surface by using the physical optics (i.e., Kirchhoff approximation) as already proposed in [7, 23]. Thus, the sea surface plus the target can be seen as a single target for our model.

In the following, the generation of a realistic sea surface (geometry and electrical parameters) is detailed. Then, some numerical results are proposed to illustrate the proposed approach.

3.1. Sea surface model

The scattering properties of the sea depend both on its electromagnetic characteristics and its state (geometrical aspect). The geometric properties of the sea surface can be modeled as a random height as a function of the position (x, y) and time t. The power spectral density of the wave height S is generally given by

$$S(\vec{K}) = \frac{1}{K} S_1(K) S_2(\psi), \tag{4}$$

where $\vec{K}$ is the sea wave vector, K the norm of $\vec{K}$, S_1 is the omnidirectional wave height spectrum and S_2 the spread function. ψ is the difference between the direction of the waves and the direction of the wind.

To generate a realistic sea surface, the Elfouhaily spectrum [24] has been used. It has been developed from the work of Pierson [25]

combined with experimental measurements. This model was developed solely from in situ or tank measurements, along with physical arguments however it also agrees with the slope model proposed by Cox and Munk and with actual remote sensing data. The directional wave height spectrum is that proposed by Fung and Lee [26].

Figure 12 shows an example of a sea surface. The sea parameters used have been fixed at 5 m/s for the wind speed at 19.5 m, 25° for the wind direction, 0° for the direction of the wave propagation and the omnidirectional Elfouhaily spectrum.

From the high frequency point of view, if the rough surface has a large curvature radius, the physical optics approximation will obviously be very good when the reflection from rough surface is evaluated [23, 27]. To compute the scattered field, the sea surface generated from the sea spectrum is also meshed by triangular facets.

The electromagnetic characteristics of the sea are defined by the dielectric constant which depends on the temperature and the salinity [28].

Notice that the interaction between the target and the sea surface can be considered as double bounce. Figure 13 shows the interactions considered in our RCS computation.

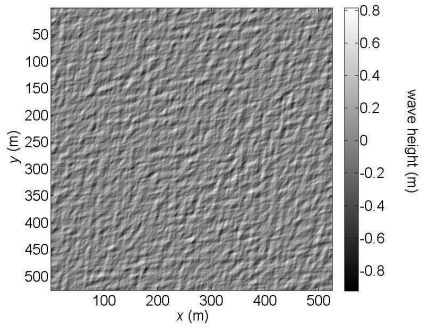

Figure 12. Generated deterministic sea surface.

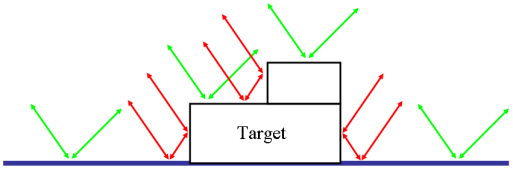

Figure 13. Considered interactions between the incident field and the scene composed of a target on a surface.

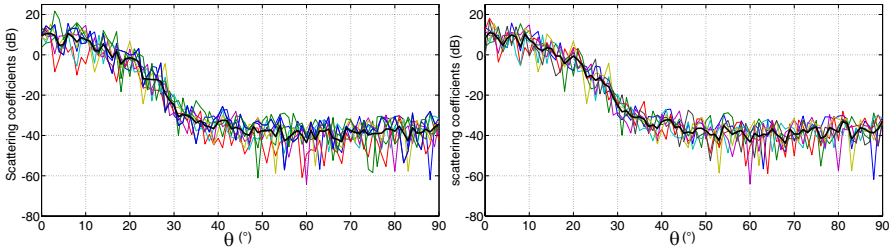

Figure 14. Monostatic RCS of a deterministic sea surface generated 10 times (a) *hh*-polarization, (b) *vv*-polarization. The thick line corresponds to the average of all the obtained RCS.

3.2. Kirchhoff Approximation and Small-perturbation Model Versus Optical Physics for Deterministic Surfaces

To compute the scattered field from a sea surface, various methods can be used (numerical methods such as the method of moments, the approximate methods or statistical-based approaches). In this contribution deterministic surface is considered and the scattered field from the discretized surface is computed using physical optics. Notice that physical optics does not give access to the cross-polarization.

Figure 14 shows the RCS of 10 sea surface (512×512) m-sized generated with the same parameters: wind speed $= 5\,\mathrm{m/s}$, wind direction $= 25°$, salinity $= 35\,\mathrm{ppt}$, temperature $= 20°\mathrm{C}$ and direction of the wave propagation $= 0°$. The thick line corresponds to the average of all RCS.

We propose a comparison of these results with the common Kirchhoff Approximation (KA) computed from slope distributions and the Small-Perturbation Model (SPM).

3.2.1. Kirchhoff Approximation

The KA model is known to be adequate to compute the average specular component for gravity waves, which satisfy the large curvature condition, and for an infinite sea. Basically, the scattering coefficients σ_{mn} (m and n stand for the h or v polarization) are proportional to the probability of finding specular points on a lighted surface:

$$\sigma_{mn} = \frac{\pi k^2 ||\vec{q}||^2}{q_z^4} |U_{mn}|^2 \mathrm{Pr}(Z_x, Z_y), \tag{5}$$

where $\vec{q} = k(\hat{k}_s.\hat{k}_i) = [q_x, q_y, q_z]$, U_{mn} is a polarimetric parameter depending on the configuration angles (θ_E, φ_E, θ_R, φ_R) and on

Fresnel coefficients [29]; and $\Pr(Z_x, Z_y)$ is the probability of finding a slope $Z_x = -q_x/q_z$ and $Z_y = -q_y/q_z$ on the sea surface. The slope probability function was determined empirically and fitted to an analytical curve by Cox and Munk [30].

3.2.2. Small-perturbation Model

The SPM was introduced for radio waves by Rice [31]. It is used to obtain the scattering coefficients of a slightly rough surface as its vertical roughness scale is small compared to the transmitted wavelength and so is the surface slope. The SPM has been recently extended to the bistatic case for sea applications in [32].

Basically, the first-order scattering coefficients for a slightly rough surface with surface standard deviation σ_r are given by

$$\sigma_{mn} = 8\sigma_r^2 k^4 \cos^2(\theta_E)\cos^2(\theta_R)|\alpha_{mn}|^2 W(k_x + k\sin\theta_E, k_y), \quad (6)$$

where α_{mn} is a polarimetric coefficient that depends on the bistatic angles and the sea permittivity [33]. W is the normalized roughness spectrum that is the Fourier transform of the surface correlation coefficient. $k_x = -k\sin\theta_R\cos\varphi_R$ and $k_y = -k\sin\theta_R\sin\varphi_R$.

3.2.3. Numerical Analysis

In Figure 15, the obtained monostatic results from the three approaches (KA, SPM and PO for deterministic sea surfaces) and for both polarizations are compared. The physical optics result (average of all the RCS in Figure 14) seems to show good accuracy between the specular diffraction (KA) and the diffuse component (SPM) of rough surfaces.

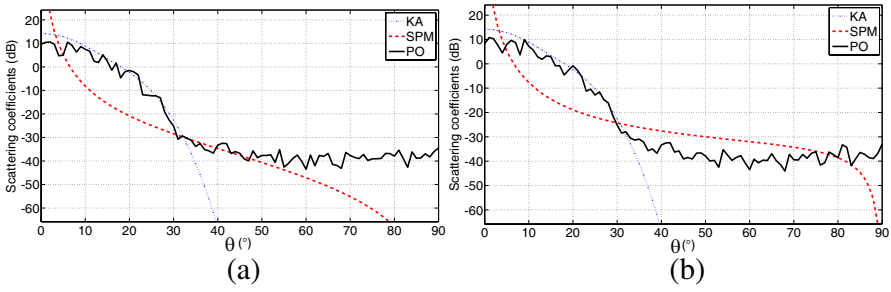

Figure 15. Monostatic RCS of the sea surface. KA and SPM versus PO (same as the thick line in Figure 14) (a) *hh*-polarization, (b) *vv*-polarization.

Notice that an equivalent study can be made in the bistatic case. In this paper, we have chosen only to show the monostatic part.

3.3. Numerical Results

3.3.1. Monostatic RCS of a Cube on a Flat PEC Surface

The considered setup corresponds to that proposed in [10] and it is depicted in Figure 16. The considered frequency is 10 GHz, both the cube and the surface are assumed to be perfectly conducting and the antenna (emitter plus receiver) moves along ($\varphi = 0°$, $\theta = 0°$ to $90°$).

The obtained results are compared with those obtained using FEKO in Figure 17. These RCS results, for both the *vv*-polarization and the *hh*-polarization, show good agreement of our model with the MoM method in this simple case.

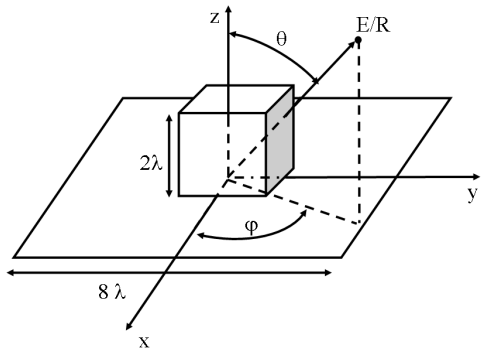

Figure 16. Configuration for a cube on a flat surface.

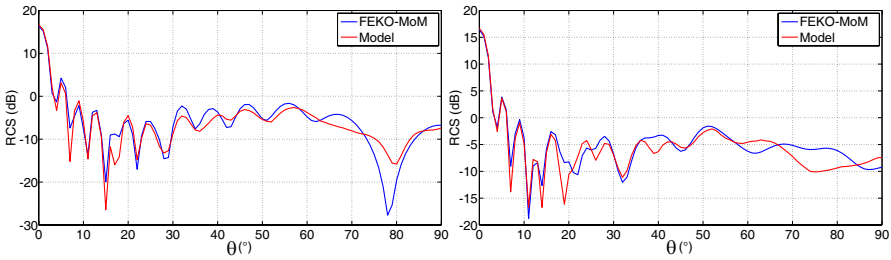

Figure 17. RCS of a PEC cube on a PEC flat surface (a) *vv*-polarization, (b) *hh*-polarization.

3.3.2. RCS of an Object on a Rough Surface

The considered setup is composed of a 0.9 m cube target on a (10×10) m rough surface (see Figure 18). This setup is based on that proposed in [7]. Notice that because of the size of the considered scene, a scale factor (equal to 10 along the x and y-axis) has been applied to the generated sea surface so that it matches the size of the object (i.e., the 10 m square rough surface has been created from a 100 m square sea surface of level 3 — see Figure 18). The sea surface has been generated following Section 3.1.

Figure 19 shows the obtained monostatic results at 1GHz for a flat PEC surface, a flat sea surface and a rough sea surface for both polarizations. The antenna move along $\varphi = 0°$ and $\theta = 0°$ to 90°. Note that, for this configuration, the fast multipole method processing (FMP) of FEKO has been used to reduce the computational time.

Figure 20 shows the obtained bistatic. For this configuration, the emitter is fixed at ($\varphi_E = 0°$, $\theta_E = 45°$) and the receiver moves along $\varphi_R = 0°$ and $\theta_R = 0°$ to 90°. The RCS obtained using FEK0 (FMP) for a PEC cube on a flat PEC surface are also presented.

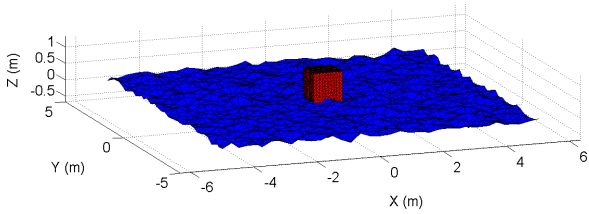

Figure 18. Cube on a rough surface.

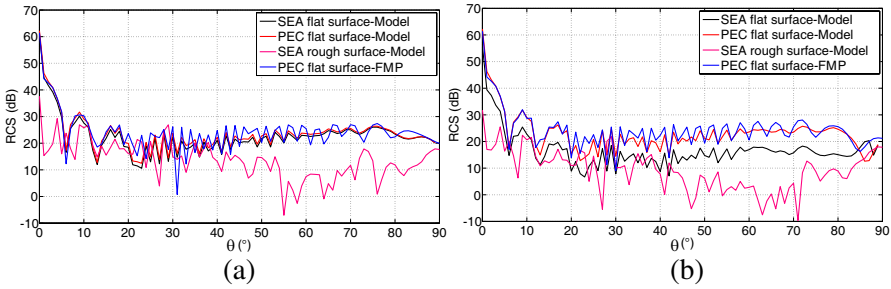

Figure 19. Monostatic RCS of a PEC cube on a flat PEC surface, a flat sea surface and a rough surface for (a) the vv-polarization and (b) the hh-polarization.

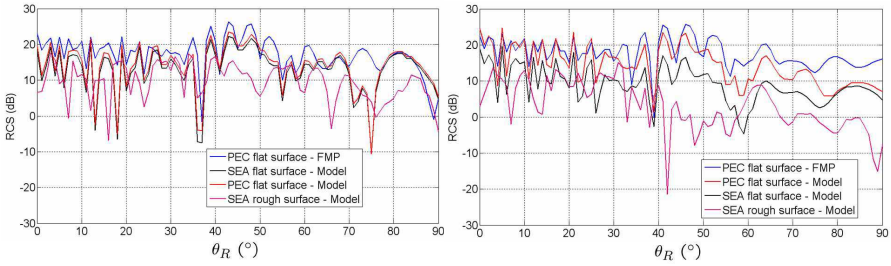

Figure 20. Bistatic RCS of a PEC cube on different surfaces for (a) the *vv*-polarization and (b) the *hh*-polarization.

These results show the evolution of the RCS considering different kinds of surface. These changes will have consequences on detection or imaging results.

4. SAR IMAGES OF MARITIME SCENES

In this part, we introduce a first use of the proposed model for generating simulated raw data for synthetic aperture radar applications (see Figure 1). Some first imaging results, for a monostatic configuration and a bistatic configuration, dealing with targets floating on a sea surface are provided.

4.1. Radar Radio-link

Following [15], the detected voltage at a given time t is

$$V(t) = \sum_{i=1}^{N_f} \frac{E_0 S_e(t - \delta t_{EC_iR}(t))}{c^2 \delta t_{EC_i}(t) \delta t_{C_iR}(t)} E_{s,i}(t), \tag{7}$$

where N_f is the number of facets and edges of the scene, E_0 is the field amplitude, $S_e(t)$ the transmitted wave form (a chirp in this paper), $\delta t_{EC_i}(t)$ the propagation delay between the emitter and the ith facet/edge of the scene, $\delta t_{C_iR}(t)$ the propagation delay between the facet/edge i and the receiver, and $\delta t_{EC_iR}(t)$ the propagation delay between the emitter, the facet/edge i and the receiver. $E_{s,i}$ is the scattered field by the ith (illuminated) facet/edge of the scene and computed following the proposed PO/MEC-based model.

Notice that, for simplicity, in this first work, antenna radiations and multiple-bounce are not taken into account (for more

computational efficiency). Moreover, one assumes the considered scene (boat floating on the sea surface) to be immobile throughout the acquisition.

4.2. Chirp Scaling Algorithm (Short Overview)

Various algorithms can be used to construct the image of the considered scene from the raw data. In this contribution, a chirp scaling-based algorithm is considered [34]. The basic block diagram is depicted in Figure 21.

4.3. Numerical Results

For all the proposed results in this section, the same radar parameters have been used. They are given in Table 1, where F_c is the central frequency, B the bandwidth, τ the chirp duration and PRF the pulse repetition frequency.

The positions and velocities of the transmitter and the receiver for a monostatic and a bistatic configurations are given in Table 2. The sea surface and the target are centered on (0; 0; 0). The direction of the target (if needed) is given by θ_b (see Figure 1).

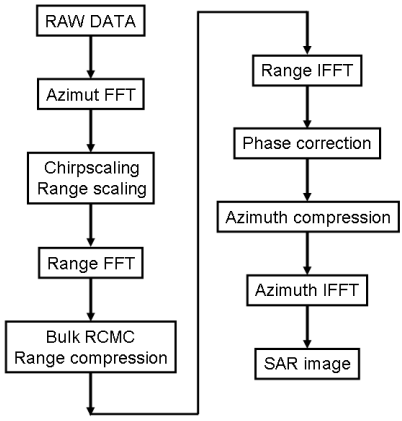

Figure 21. Block diagram of the chirp scaling algorithm.

Table 1. Radar parameters.

E_0	F_c	B	PRF	τ
1 W	10 GHz	60 MHz	800 Hz	0.333 µs

Table 2. Emitter and receiver positions and velocities — Cartesian coordinates $(x; y; z)$.

	Monostatic	Bistatic
Transmitter: Start	$(-3000; -100; 3000)$ m	$(-3000; -100; 3000)$ m
Transmitter: Stop	$(-3000; 100; 3000)$ m	$(-3000; 100; 3000)$ m
Transmitter velocity	$(0; 222; 0)$ m/s	$(0; 222; 0)$ m/s
Receiver: Start	$(-3000; -100; 3000)$ m	$(-4000; -100; 3000)$ m
Receiver velocity	$(0; 222; 0)$ m/s	$(0; 222; 0)$ m/s

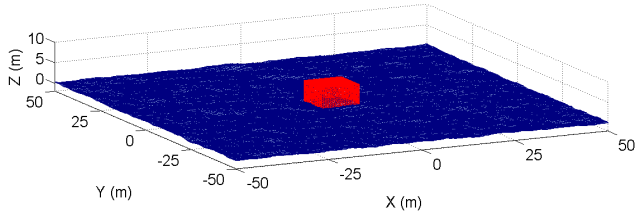

Figure 22. Box on a sea surface.

4.3.1. Scenario 1

In this configuration, we consider a canonical target on a sea surface. The object is a box with 10m sides and the sea is a (100×100) m surface. It has been generated for a wind speed equal to 5 m/s. The box is semi-immersed as shown in Figure 22.

Figures 23 and 24 shows the SAR images of the target on the sea surface for both polarizations. The cube and its shadow are clearly visible in these images. They are also illustrating the different information obtained from the monotatic and bistatic configurations.

4.3.2. Scenario 2

For that scenario, the considered scene is composed of a simplified boat on a (100×100) m-sized sea surface (see Figure 25). The geometry and the dimensions of the boat are given in Figure 26.

The monostatic (see Tables 1 and 2) SAR results are proposed for $\theta_b = 180°$, $\theta_b = 225°$, $\theta_b = 270°$. Figure 27 shows all the results. In these images, one can clearly see the shadow made by the boat. Unfortunately the boat itself cannot really be seen. This can be explained by the geometry of the boat and the considered acquisition configuration, and above all by the fact that the multiple reflections

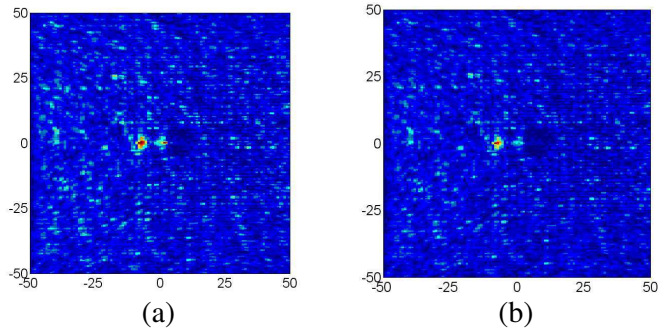

Figure 23. Monostatic SAR images of a PEC box on a sea surface (a) the *vv*-polarization and (b) the *hh*-polarization.

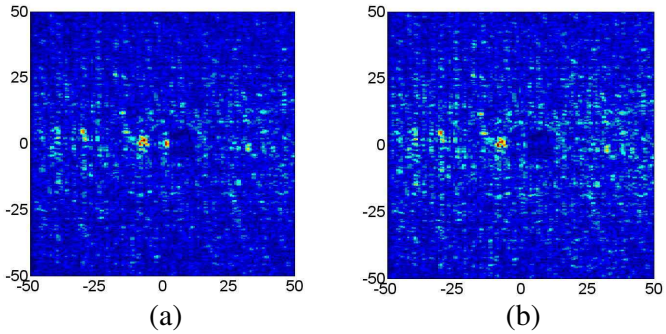

Figure 24. Bistatic SAR images of a PEC box over a sea surface (a) the *vv*-polarization and (b) the *hh*-polarization.

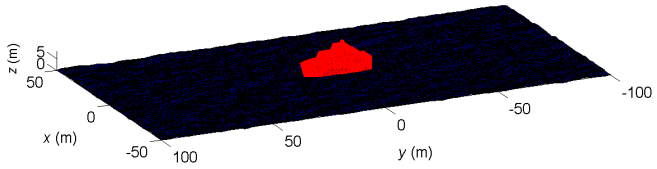

Figure 25. Scenario 2: boat (see Figure 26) floating on a sea surface.

have not been considered to avoid indiscriminate computational time. This must be tackled in future work for example by pre-processing the possible multiple-bounce rays.

The last remark is that finally this kind of model for generating SAR raw data from a three-dimensional maritime scene can be of interest from the modeling point of view.

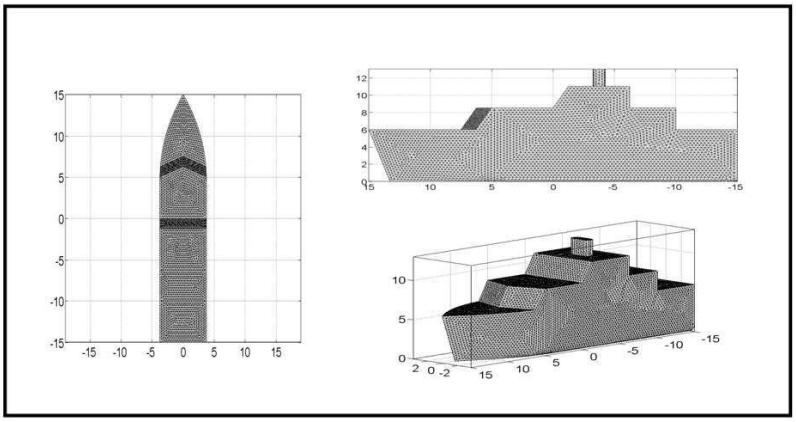

Figure 26. Boat dimensions.

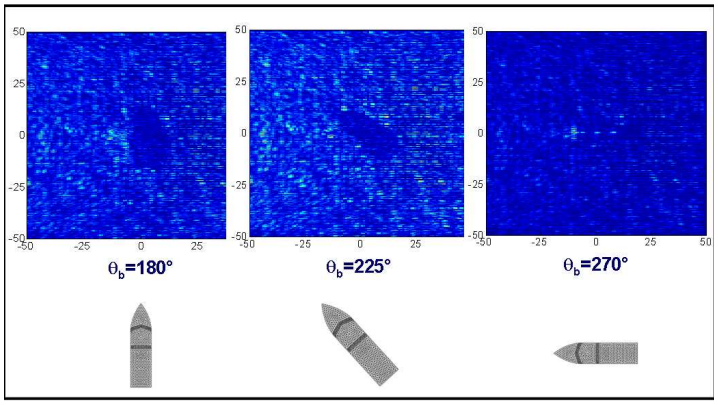

Figure 27. Monostatic SAR images of various orientations of a boat floating on a sea surface.

5. CONCLUSION

In this paper, a model to compute the scattered field from a maritime scene composed of a target on a deterministic sea surface has been proposed. The model combines asymptotic methods and takes into account shadowing effects and multiple-bounce up to order 3. Numerical RCS comparisons with results obtained from FEKO show the proposed model to have enough accuracy for our purpose.

From the model, raw data have been generated and radar images

have been obtained using a chirp scaling-based technique. The obtained results for a canonical target and a complex target show the feasibility of this kind of global SAR model for complex scenes.

Of course a number of studies can be made to enhance the proposed model. Future work will particularly focus on the model to improve its accuracy using realistic experiments. For radar imaging, the introduction of a moving sea surface and a moving target, and the bistatic configuration must be studied. Finally, computational efficiency has to be carefully considered.

REFERENCES

1. Hazlett, M., D. Andersh, and S. Lee, "XPATCH: A high frequency electromagnetic scattering prediction code using shooting and bouncing rays," *SPIE*, Vol. 2469, 266–275, 1999.
2. Rius, J., M. Ferrando, and L. Jofre, "GRECO: Graphical electromagnetic computing for RCS prediction in real time," *IEEE Antennas and Propagation Magazine*, Vol. 35, No. 2, 7–17, 1993.
3. Keller, J., "Geometrical theory of diffraction," *Journal of the Optical Society of America*, Vol. 52, 116–130, 1962.
4. Knott, E., J. Shaeffer, and M. Tuley, *Radar Cross Section*, 2nd edition, SciTech Publishing, 2004.
5. Michaeli, A., "Equivalent edge currents for arbitrary aspect of observation," *IEEE Trans. on Antennas and Propagation*, Vol. 32, No. 3, 252–258, 1984.
6. Ufimtsev, P., "Method of edge waves in the physical theory of diffraction," (in translation from the Russian version published by Soviet Radio Publication House, Moscow, 1962), Tech. Rep. Document ID FTD-HC-23-259-71, Air Force Systems Command, Foreign Tech., 1971.
7. Burkholder, R., P. Janpugdee, and D. Colak, "Development of computational tools for predicting the radar scattering from targets on a rough sea surface," Tech. Rep. 735231-3, ElectroScience Lab, The Ohio State University, 2001.
8. Kim, K., J.-H. Kim, and D.-S. Cho, "Radar cross section analysis of marine targets using a combining method of physical optics/geometric optics and a monte-carlo simulation," *Ocean Engineering*, Vol. 36, No. 11, 821–830, 2009.
9. Luo, W., M. Zhang, Y.-W. Zhao, and H. Chen, "An efficient hybrid high-frequency solution for the composite scattering of the ship very large two-dimensional sea surface," *Progress In Electromagnetics Research M*, Vol. 8, 79–89, 2009.

10. Xu, F. and Y.-Q. Jin, "Bidirectional analytic ray tracing for fast computation of composite scattering from electric-large target over a randomly rough surface," *IEEE Trans. Antennas and Propagation*, Vol. 57, No. 5, 1495–1505, 2009.
11. Ye, H. and Y.-Q. Jin, "Fast iterative approach to difference scattering from the target above a rough surface," *IEEe Trans. Geoscience and Remote Sensing*, Vol. 44, No. 1, 108–115, 2006.
12. Mishra, A. and B. Mulgrew, "Generation of sar image for real-life objects using general purpose em simulators," *IETE Technical Review*, Vol. 26, No. 1, 18–27, 2009.
13. Margarit, G., J. Mallorqui, J. Rius, and J. Sanz-Marcos, "On the usage of grecosar, an orbital polarimetric sar simulator of complex targets, to vessel classification studies," *IEEE Trans. Geoscience and Remote Sensing*, Vol. 44, No. 12, 3517–3526, 2006.
14. Auer, S., S. Hinz, and R. Bamler, "Ray-tracing simulation techniques for understanding high-resolution SAR images," *IEEE Trans. Geoscience and Remote Sensing*, Vol. 48, No. 3, 1445–1456, 2010.
15. Airiau, O. and A. Khenchaf, "A methodology for modeling and simulating target echoes with a moving polarimetric bistatic radar," *Radio Science*, Vol. 35, No. 3, 773–782, 2000.
16. Comblet, F., A. Khenchaf, A. Baussard, and F. Pellen, "Bistatic synthetic aperture radar imaging: Theory, simulations, and validations," *IEEE Trans. Antennas and Propagation*, Vol. 54, No. 11, 3529–3540, 2006.
17. Arnold-Bos, A., A. Khenchaf, and A. Martin, "Bistatic radar imaging of the marine environment. Part I: Theoretical background," *IEEE Trans. on Geoscience and Remote Sensing*, Vol. 45, No. 11, 3372–3383, 2007.
18. Arnold-Bos, A., A. Khenchaf, and A. Martin, "Bistatic radar imaging of the marine environment. Part II: Simulation and results analysis," *IEEE Trans. on Geoscience and Remote Sensing*, Vol. 45, No. 11, 3384–3396, 2007.
19. Dos Santos, M. and N. Rabelo, "On the ludwig integration algorithm for triangular subregions," *IEEE Proceedings*, No. 10, 1986.
20. Michaeli, A., "Elimination of infinities in equivalent edge current. Part 1: Physical optics components," *IEEE Trans. on Antennas and Propagation*, Vol. 34, No. 8, 1034–1037, 1986.
21. Michaeli, A., "Elimination of infinities in equivalent edge currents, part II: Physical optics components," *IEEE Trans. on Antennas*

and Propagation, Vol. 34, No. 8, 1034–1037, 1986.

22. Polycarpou, A., C. Balanis, and P. Tirkas, "Radar cross section evaluation of the square trihedral corner reflector using PO and MEC," *IEEE International Antennas and Propagation Symposium*, Vol. 3, 1428–1431, 1993.
23. Burkholder, R. and K. Jamil, "Simulation of electromagnetic scattering experiments in the NSWC Carderock MASK facility," Tech. Rep. 742961-1, 2003.
24. Elfouhaily, T., B. Chapron, and K. Katsaros, "A unified directional spectrum for long and short," *Journal of Geophysical Research*, Vol. 102, No. C7, 15–781, 1997.
25. Pierson, W. and L. Moskowitz, "A proposed spectral form for fully developed wind seas based upon the similarity theory of s.a. Kitaigorodskii," *Journal of Geophysical Research*, Vol. 69, 5181–5190, 1964.
26. Fung, A. K. and K. K. Lee, "A semi-empirical sea-spectrum model for scattering coefficient estimation," *IEEE Journal of Oceanic Engineering*, Vol. 7, No. 4, 166–176, 1982.
27. Cao, Q.-F., S. Liu, and P.-G. Xu, "SCTE: RCS prediction system for complex target and interaction with environment," *Wuhan University Journal of Natural Sciences*, Vol. 4, No. 3, 299–203, 1999.
28. Klein, L. and C. Swift, "An improved model for the dielectric constant of sea water at microwave frequencies," *IEEE Trans. on Antennas and Propagation*, Vol. 25, No. 1, 104–111, 1977.
29. Ulaby, F. T., R. K. Moore, and A. K. Fung, *Microwave Remote Sensing: Active and Passive*, Vol. 2, Artech House, 1986.
30. Cox, C. and W. Munk, "Statistics of the sea surface derived from sun glitter," *Journal of Marine Research*, Vol. 13, 198–227, 1954.
31. Rice, S., "Reflection of electromagnetic waves from slightly rough surfaces," *Theory of Electromagnetic Waves*, 351–378, 1951.
32. Khenchaf, A. and O. Airiau, "Bistatic radar moving returns from sea surface," *IEICE Trans. on Electronics*, Vol. E83-C, No. 12, 1827–1835, 2000.
33. Ishimaru, A., *Wave Propagation and Scattering in Random Media*, Academic Press, 1978.
34. Moreira, A., J. Mittermayer, and R. Scheiber, "Extended chirp scaling algorithm for air- and spaceborne SAR data processing in stripmap and scansar imaging modes," *IEEE Trans. on Geoscience and Remote Sensing*, Vol. 34, No. 5, 1123–1136, 1996.